Int. J. Heat Mass Transfer. Vol. 10, pp. 597–610. Pergamon Press Ltd. 1967. Printed in Great Britain

THEORETICAL RESULTS FOR VARIABLE PROPERTY, LAMINAR BOUNDARY LAYERS IN WATER

G. POOTS and G. F. RAGGETT
Department of Applied Mathematics, The University of Hull

(*Received* 15 *July* 1966 *and in revised form* 24 *October* 1966)

Abstract—Numerical solutions are presented for laminar forced heat convection in water for two different laminar boundary layer flow configurations. Experimental values (in the range 0–100°C) for the viscosity conductivity, specific heat and density are used. First the laminar forced convection heat transfer from a semi-infinite flat plate to a parallel stream is examined. Secondly the heat transfer by laminar flow about an infinite rotating disk is analysed. It is assumed that viscous dissipation, work done against compression and the gravitational buoyancy force are negligible. The relevant boundary-layer equations are solved numerically for isothermal plate (or disk) conditions.

Flow and heat-transfer properties of these solutions, for both flow régimes, are given in graphical and tabular form for several combinations of plate and free stream temperatures. The theoretical results for the wall Nusselt number are correlated by expressions of the type $Nu/Re^{\frac{1}{2}} = A\,Pr_w^{\alpha}\,Pr_m^{\beta}$, where Re is the Reynolds number, Pr is the Prandtl number and the subscripts m and w indicate that main stream and wall fluid property values are taken. Consideration is also given to the use of effective reference temperatures at which fluid properties should be evaluated when a constant fluid property model is employed to determine wall heat-transfer coefficients.

NOMENCLATURE

A_i, B_i, C_i, D_i, coefficients [see equation (1.1)];
a, radius of curvature [cm];
c_p, specific heat at constant pressure [cal/g degC];
C_f, dimensionless skin friction coefficient;
C_M, dimensionless moment coefficient for the disk;
E_m, $= u_m^2/Jc_{p_m}(T_w - T_m)$, Eckert number;
f, g, h, dimensionless velocity functions;
Gr, $= g\rho(\rho_w - \rho)x^3/\mu^2$, Grashof number;
k, thermal conductivity [cal/cm s degC];
M, torque on disk;
Nu, Nusselt number;
p, pressure;
P, dimensionless pressure;
Pr, $= c_p\,\mu/k$, Prandtl number;
q, local heat flux;
Q, mass flow per second;
Re, $= \rho u_m x/\mu$, Reynolds number;
r, θ, z, cylindrical polar coordinates;
T, temperature [°C];
u, v, velocity components for the plate [cm/s];
u_r, u_θ, u_z, velocity components for the disk [cm/s];
x, y, Cartesian co-ordinates;
Y, $= \int_0^y \frac{\rho}{\rho_m}\,dy$, Howarth–Dorodnitsyn y-variable [see equation (2·9b)];
R, Z, dimensionless r, z variables for the disk.

Greek symbols

γ, constant;

$\delta_1, \delta_2, \delta_3$, boundary-layer thicknesses for the plate [see equations (2.19) to (2.21)];

$\Delta_1, \Delta_2, \Delta_3$, boundary-layer thicknesses for the disk [see equations (3.12) to (3.14)];

μ, viscosity, [g/cm s];

ϵ, angle between resultant velocity and zonal direction for the disk;

$\tau_w, \tau_{z\theta}$, shear stresses;

Ω, angular velocity [rad/s];

θ, $= (T - T_w)/(T_m - T_w)$, dimensionless local temperature;

Θ, $= (T - 50°C)/50°C$, dimensionless scaled temperature;

ρ, density [g/cm^3];

η, $= Y\left(\frac{\rho_m u_m}{2\mu_m x}\right)^{\frac{1}{2}} \int_0^Z \frac{\rho}{\rho_m} dZ$, dimensionless independent variables for the plate and disk [as in equations (2.9a) and (3.2), respectively];

ψ, stream function.

Subscripts

f, liquid film condition;

m, main stream;

w, wall condition;

r, reference condition.

1. INTRODUCTION

SEVERAL theoretical studies now exist on the determination of local and average heat-transfer coefficients in liquids taking into account the effect of variable viscosity. The major portion of this work dealt with non-isothermal forced convection flow inside vertical tubes. A brief survey was given in Poots and Rogers [1]. In the aforementioned report the fully developed laminar forced convection to water between heated vertical flat plates was discussed in detail using experimental data (in the range 0–100°C) for the viscosity, conductivity, specific heat and density. The main effect of variable fluid properties was on the mass flow and this was primarily produced by the rapid variation of viscosity with temperature. For example, mass flow rates in the case of Couette flow evaluated using the experimental data for water differed by as much as 25 per cent from those evaluated using a constant fluid property model based on physical properties taken at the arithmetic mean temperature of the plates. Discrepancies in the case of Poiseuille flow were at most 16 per cent. However, in [1] the heat flux across the channel was constant and independent of the flow rate, and so no new information was obtained on the effects of variable viscosity, etc., on wall Nusselt numbers.

It is the purpose of this report to examine some non-isothermal laminar flows in water, where there is appreciable coupling between the momentum and thermal energy boundary-layer equations. In view of the computational difficulties incurred when due account is taken of variable physical properties it is clear that results can most easily be obtained on considering similarity solutions of these equations. Thus in Section 2, the laminar boundary-layer equations are solved for the velocity and temperature distribution in the vicinity of an isothermal flat plate aligned parallel with a uniform water stream of infinite extent for several combinations of plate and free stream temperatures. In Section 3 the rotationally symmetrical flow and heat transfer in the presence of an isothermal infinite rotating disk is examined. In both flow configurations the momentum and thermal boundary layer equations are supplemented by certain fluid property relations for the density, specific heat, viscosity and conductivity. Except at very high pressures, or at conditions near the critical point, these properties for water may be taken as equal to saturated values at the appropriate temperatures. The data for saturated values are taken from tables compiled by Mayhew and Rogers [2]. In cgs units these experimental values are adequately represented, as is discussed in [1], by algebraic expressions in the

form:

$$\rho = \sum_{i=0}^{10} A_i \Theta^i, \qquad c_p = \sum_{i=0}^{10} B_i \Theta^i,$$
$$\mu = \exp\left(\sum_{i=0}^{10} C_i \Theta^i\right), \tag{1.1}$$
$$k = \exp\left(\sum_{i=0}^{10} D_i \Theta^i\right),$$

where $\Theta = (T - 50°C)/50°C$; the numerical values of the A_i, B_i, C_i and D_i are listed in ref. [1].

2. THE BOUNDARY LAYER ON AN ISOTHERMAL FLAT PLATE

Water with uniform free stream velocity u_m and temperature T_m flows parallel to an isothermal vertical flat plate, defined by $y = 0$, $x \geqslant 0$, in the direction of increasing x; the plate temperature is T_w. Let u and v be the velocity components in the x and y directions respectively and T be the local temperature field.

The governing equations for conservation of mass, momentum and thermal energy in the resulting boundary-layer flow are, respectively:

$$\frac{\partial}{\partial x}(\rho u) + \frac{\partial}{\partial y}(\rho v) = 0, \tag{2.1}$$

$$\rho\left(u\frac{\partial u}{\partial x} + v\frac{\partial u}{\partial y}\right) = \frac{\partial}{\partial y}\left(\mu\frac{\partial u}{\partial y}\right), \tag{2.2}$$

and

$$\rho\, c_p\left(u\frac{\partial T}{\partial x} + v\frac{\partial T}{\partial y}\right) = \frac{\partial}{\partial y}\left(k\frac{\partial T}{\partial y}\right). \tag{2.3}$$

Together with the fluid property relations (1.1) the above equations (2.1) to (2.3) must be solved subject to the boundary conditions:

$$\left.\begin{aligned} &T = T_w, && u = v = 0 \\ &&& \text{at} \quad y = 0, \quad x \geqslant 0, \\ &T = T_m, && u = u_m \\ &&& \text{at} \quad x = 0, \quad y \geqslant 0, \end{aligned}\right\} \tag{2.4}$$

and

$$\left.\begin{aligned} &T \to T_m, && u \to u_m \\ &&& \text{as} \quad y \to \infty. \end{aligned}\right\}$$

In equations (2.2) and (2.3) the gravitational buoyancy force, viscous dissipation and work done against compression have been neglected. It can be shown qualitatively on examination of the full equations of motion for a viscous heat conducting compressible fluid that the effect of the gravitational buoyancy force is negligible if:

$$\frac{Gr_m}{Re_m^2} \ll 1, \tag{2.5}$$

where the Reynolds number $Re_m = \rho_m u_m x/\mu_m$, and the Grashof number $Gr_m = g\rho_m(\rho_w - \rho_m)x^3/\mu_m^2$. Similarly the effects of viscous dissipation and work done against compression are negligible if:

$$Pr_m\, E_m \ll 1, \tag{2.6}$$

where the Prandtl number $Pr_m = c_{p_m}\mu_m/k_m$, and the Eckert number $E_m = u_m^2/[Jc_{p_m}(T_w - T_m)]$. For water, under realistic flow conditions, the specifications (2.5) and (2.6) are satisfied for moderate speeds and large temperature differences.

Upon introducing a stream function ψ defined by

$$\rho u = \rho_m \frac{\partial \psi}{\partial y}, \qquad \rho v = -\rho_m \frac{\partial \psi}{\partial x}, \tag{2.7a}$$

and the dimensionless temperature distribution θ defined by:

$$\theta = \frac{T - T_w}{T_m - T_w} \tag{2.7b}$$

the required similarity solution (see, for example, Stewartson [3]) of the boundary-layer equations (2.1) to (2.3) is in the form:

$$\left.\begin{aligned} &\psi = (2\,\mu_m\, u_m\, x/\rho_m)^{\frac{1}{2}} f(\eta), \\ &\theta = \theta(\eta). \end{aligned}\right\} \tag{2.8}$$

Here η is the Blasius similarity variable defined by

$$\eta = Y\,(\rho_m\, u_m/2\,\mu_m\, x)^{\frac{1}{2}}, \tag{2.9a}$$

where Y is the Howarth–Dorodnitsyn variable:

$$Y = \int_0^y \frac{\rho}{\rho_m}\,\mathrm{d}y\,. \tag{2.9b}$$

The velocity field is related to f by:

$$\left.\begin{aligned} u &= u_m \, \mathrm{d}f/\mathrm{d}\eta \\ \text{and} \\ v &= -\frac{\rho_m}{\rho}\left\{\left(\frac{\mu_m \mu_m}{2\rho_m x}\right)^{\frac{1}{2}}\left(f - \eta\frac{\mathrm{d}f}{\mathrm{d}\eta}\right) + u_m \frac{\mathrm{d}f}{\mathrm{d}\eta}\left(\frac{\partial Y}{\partial x}\right)_y\right\}. \end{aligned}\right\} \quad (2.10)$$

Accordingly equations (2.1), (2.2) and (2.3) reduce to the following ordinary differential equations:

$$\frac{\mathrm{d}}{\mathrm{d}\eta}\left(\frac{\rho\mu}{\rho_m \mu_m}\frac{\mathrm{d}^2 f}{\mathrm{d}\eta^2}\right) + f\frac{\mathrm{d}^2 f}{\mathrm{d}\eta^2} = 0, \quad (2.11)$$

and

$$\frac{\mathrm{d}}{\mathrm{d}\eta}\left(\frac{\rho k}{\rho_m k_m}\frac{\mathrm{d}\theta}{\mathrm{d}\eta}\right) + Pr_m \frac{c_p}{c_{p_m}} f\frac{\mathrm{d}\theta}{\mathrm{d}\eta} = 0. \quad (2.12)$$

The fluid property relations (1.1) take the simple form:

$$\left.\begin{aligned} \rho &= \rho(\theta; T_w, T_m), \\ c_p &= c_p(\theta; T_w, T_m), \\ \mu &= \mu(\theta; T_w, T_m) \\ \text{and} \\ k &= k(\theta; T_w, T_m), \end{aligned}\right\} \quad (2.13)$$

where, for example:

$$\rho = \sum_{i=0}^{10} A_i \{[T_w + (T_m - T_w) \times \theta(\eta) - 50°\mathrm{C}]/50°\mathrm{C}\}^i.$$

The boundary conditions are:

$$\left.\begin{aligned} f = \mathrm{d}f/\mathrm{d}\eta = \theta = 0 \quad &\text{at} \quad \eta = 0, \\ \mathrm{d}f/\mathrm{d}\eta \to 1, \quad \theta \to 1 \quad &\text{as} \quad \eta \to \infty. \end{aligned}\right\} \quad (2.14)$$

To date (2.11), (2.12) subject to (2.14) have been solved on the basis of a constant fluid property model. It is not unreasonable to assume for quite small temperature differences, $(T_m - T_w)$, that the physical properties of the liquid are independent of the temperature. The relevant values can then be taken at a suitable reference temperature. If the free stream temperature is chosen as this reference temperature equations (2.11) and (2.12) are replaced by

$$f''' + ff'' = 0, \qquad \theta'' + Pr_m f\,\theta' = 0, \quad (2.15)$$

where the prime denotes differentiation with respect to η. Details of the classic Blasius–Pohlhausen solutions of (2.15) subject to (2.14) are given in Stewartson [3] for Prandtl numbers in the range $0{\cdot}6 \leqslant Pr_m \leqslant 15$. However, for even moderate temperature differences the use of the above type of model based on the reference temperature T_m must lead to serious errors in the prediction of liquid flow and heat-transfer characteristics. For example, in the specific case of water the Prandtl number is a monotonically decreasing function varying from 13·621 to 1·737 in the range 0–100°C. Later in this section it is shown that an accurate prediction for the wall heat-transfer coefficient may be obtained using a constant fluid property model based on an effective reference temperature deduced from the computed variable fluid property results.

Solutions

Numerical solutions of the variable property equations (2.11) to (2.14) have been obtained for $T_w = 0$, 10, 40, 70 and 100°C when T_m is either 0, 10, 40, 70 or 100°C. The integrations were performed using Gill's modification of the Runge–Kutta method. An iterative scheme was used for the determination of the unknown initial values $f''(0)$ and $\theta'(0)$; these have been rounded off to four decimals and are listed in Table 1.

Velocity and thermal profiles

Representative dimensionless velocity profiles for the extreme cases $(T_w, T_m) = (100, 0)$, (0, 0), (100, 100) and (0, 100) are given in Fig. 1; the associated temperature profiles are given in Fig. 2. As the similarity variable η is defined using the reference temperature T_m it is only

Table 1

T_w	T_m	$f''(0)$	$\theta'(0)$	$\delta_1 Re_m^{\frac{1}{2}}/x$	$\delta_2 Re_m^{\frac{1}{2}}/x$	$\delta_3 Re_m^{\frac{1}{2}}/x$	$Nu/Re_m^{\frac{1}{2}}$	$C_f Re_m^{\frac{1}{2}}$	$Nu/C_f Re_m$
0	0	0·4696	1·1421	1·7208	0·6641	1·0444	0·8076	0·6641	1·2161
10		0·6218	1·1916	1·5699	0·6442	1·0214	0·8425	0·6442	1·3080
40		1·1169	1·3194	1·2208	0·5743	0·9342	0·9258	0·5743	1·6122
70		1·6041	1·4361	0·9870	0·5032	0·8364	0·9929	0·5032	1·9732
100		2·0567	1·5534	0·8265	0·4396	0·7427	1·0523	0·4396	2·3940
0	10	0·3533	0·9757	1·8767	0·6820	1·0646	0·6900	0·6820	1·0117
10		0·4696	1·0130	1·7208	0·6641	1·0444	0·7163	0·6641	1·0786
40		0·8557	1·1157	1·3585	0·6006	0·9665	0·7829	0·6006	1·3036
70		1·2469	1·2124	1·1121	0·5339	0·8768	0·8383	0·5339	1·5702
100		1·6195	1·3117	0·9404	0·4725	0·7884	0·8886	0·4725	1·8808
0	40	0·1869	0·7001	2.2673	0·7269	1·1172	0·4989	0·7269	0·6863
10		0·2505	0·7196	2·1066	0·7137	1·1028	0·5127	0·7137	0·7183
40		0·4696	0·7753	1·7208	0·6641	1·0444	0·5482	0·6641	0·8255
70		0·7046	0·8358	1·4466	0·6079	0·9724	0·5823	0·6079	0·9578
100		0·9401	0·9016	1·2491	0·5526	0·8968	0·6155	0·5526	1·1138
0	70	0·1198	0·5645	2·5589	0·7637	1·1624	0·4083	0·7637	0·5346
10		0·1613	0·5744	2·4007	0·7534	1·1514	0·4154	0·7534	0·5513
40		0·3075	0·6070	2·0090	0·7128	1·1048	0·4356	0·7128	0·6111
70		0·4696	0·6478	1·7208	0·6641	1·0444	0·4581	0·6641	0·6897
100		0·6370	0·6957	1·5066	0·6138	0·9780	0·4820	0·6138	0·7853
0	100	0·0851	0·4811	2·7803	0·7963	1·2037	0·3551	0·7963	0·4459
10		0·1149	0·4855	2·6279	0·7878	1·1949	0·3583	0·7878	0·4548
40		0·2215	0·5046	2·2400	0·7535	1·1562	0·3696	0·7535	0·4905
70		0·3423	0·5335	1·9452	0·7104	1·1039	0·3850	0·7104	0·5419
100		0·4696	0·5689	1·7208	0·6641	1·0444	0·4023	0·6641	0·6058

permissible to compare profiles with the same Reynolds number Re_m.*

For the two velocity profiles specified by $T_m = 0°C$ and $T_w = 0$ and 100°C, respectively, it is obvious that as the plate is heated (or as T_w increases) the coefficient of viscosity will be reduced in that part of the boundary layer close to the wall. The tangential shear stress exerted by the plate on the adhering layer of fluid is decreased producing an increase in the velocity component parallel to the plate (see Fig. 1). Quantitative information on these trends is also available in Table 1. For $T_m = 0°C$ an increase in T_w results in an increase in $f''(0)$ producing a steeper velocity profile and in fact there is, as expected, a corresponding decrease in the skin friction coefficient

$$C_f Re_m^{\frac{1}{2}} = \mu_w \left(\frac{\partial u}{\partial y}\right)_{y=0} \Big/ (\tfrac{1}{2}\rho_m u_m^2).$$

An increase in velocity enhances heat transfer by convection producing the observed increase in the dimensionless temperature profiles for $(T_w, T_m) = (100, 0)$ and $(0, 0)$ as shown in Fig. 2.

In the second two velocity profiles with $T_m = 100°C$ and $T_w = 0$ and 100°C, respectively, cooling the wall obviously produces a decrease

* Of course the velocity profiles given in Fig. 1 can be plotted against an η_r based on a different reference temperature T_r, where η_r is $\eta_m(\rho_m\mu_m/\rho_r\mu_r)^{\frac{1}{2}}$. If, for example, T_w is chosen as this reference temperature then the difference between the variable fluid property profile and the related constant fluid property profile (when $T_w = T_m$) becomes much smaller near the wall than that which occurs in Fig. 1, but becomes larger at the outer edge of the boundary layer. Even if effective reference temperatures are introduced no real advantages are to be gained in the graphical representation of the results.

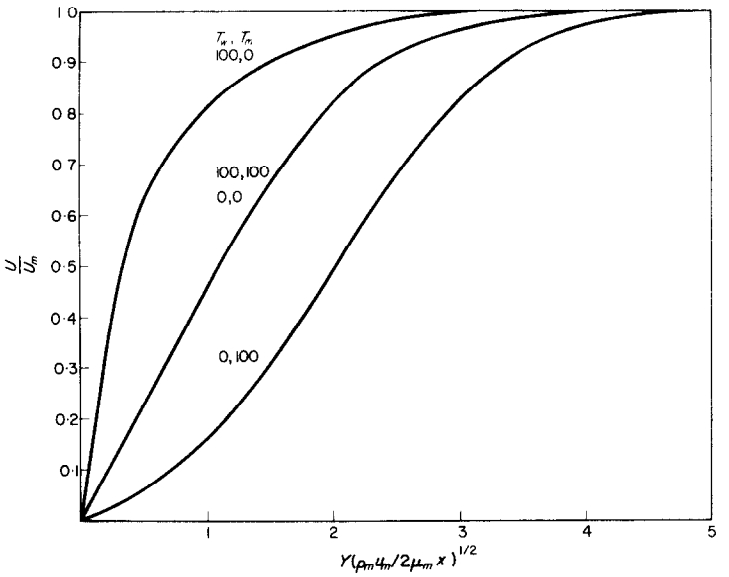

FIG. 1. Dimensionless velocity profiles for the flat plate.

in velocity as implied by the fact that the shear stress exerted by the plate increases with decreasing temperature.

Again from Fig. 2 it follows that, for flows with the same Re_m, the thermal boundary-layer thickness decreases with heating the plate.

It is, perhaps, interesting to point out that a heated wall velocity profile, as in the case $T_w = 100$ and $T_m = 0$ shown in Fig. 1, resembles closely the shape of the velocity profile occurring in an isothermal two-dimensional boundary layer with favourable pressure gradient. Similarly a cooled wall velocity profile, as in the case $T_w = 0$ and $T_m = 100$ shown in Fig. 1, resembles the type of velocity profile occurring in an isothermal two-dimensional boundary layer with an adverse pressure gradient. Moreover, in the cooled wall profile there is a point of inflexion indicating that this flow is probably unstable even at large Reynolds number.

Boundary-layer thickness

It is useful to consider some overall measures of the fluid boundary-layer thickness. These are the displacement thickness:

$$\delta_1 = \int_0^\infty \left(1 - \frac{\rho u}{\rho_m u_m}\right) dy, \qquad (2.16)$$

the momentum thickness:

$$\delta_2 = \int_0^\infty \frac{\rho u}{\rho_m u_m}\left(1 - \frac{u}{u_m}\right) dy, \qquad (2.17)$$

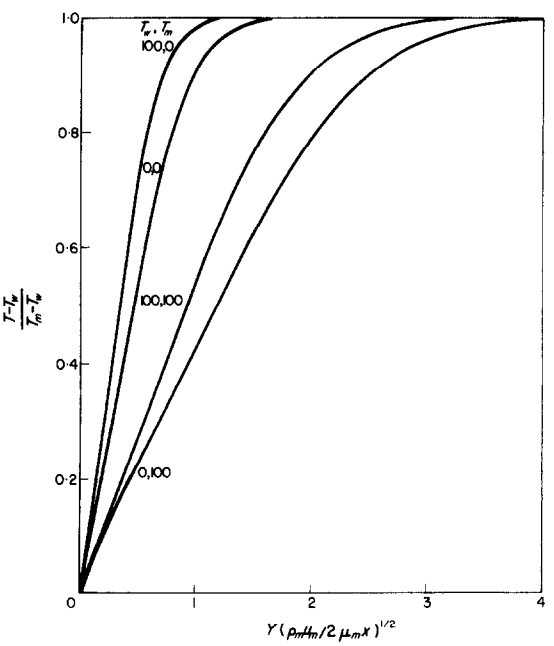

FIG. 2. Dimensionless thermal profiles for the flat plate.

and the energy thickness:

$$\delta_3 = \int_0^\infty \frac{\rho u}{\rho_m u_m}\left(1 - \frac{u^2}{u_m^2}\right) \mathrm{d}y. \qquad (2.18)$$

In terms of the new variables f and θ in the (x, η) plane the above quantities are transformed to dimensionless form as follows:

$$\frac{\delta_1 Re_m^{\frac{1}{2}}}{x} = (\sqrt{2})\int_0^\infty \frac{\rho_m}{\rho}\left(1 - \frac{\rho}{\rho_m} f'\right) \mathrm{d}\eta, \qquad (2.19)$$

$$\frac{\delta_2 Re_m^{\frac{1}{2}}}{x} = (\sqrt{2})\frac{\rho_w \mu_w}{\rho_m \mu_m} f''(0), \qquad (2.20)$$

and

$$\frac{\delta_3 Re_m^{\frac{1}{2}}}{x} = (\sqrt{2})\int_0^\infty f'[1 - (f')^2] \mathrm{d}\eta. \qquad (2.21)$$

Note that the expression for $\delta_2 Re_m^{\frac{1}{2}}/x$ as given in (2.20) is derived from the definition (2.17) by making use of the differential equation (2.11). As in the constant fluid property flow model this result shows that there is a simple relationship between the momentum thickness δ_2 and the skin friction coefficient C_f, namely, $\delta_2 = C_f x$.

Numerical values of $\delta_1 Re_m^{\frac{1}{2}}/x$, $\delta_2 Re_m^{\frac{1}{2}}/x$ and $\delta_3 Re_m^{\frac{1}{2}}/x$ are given in Table 1, and also in graphical form in Fig. 3 for the extreme cases $T_m = 0$ and 100°C. All these quantities have the same general trend, i.e. for fixed Re_m (or T_m) they decrease with increasing plate temperature.

The deficit in the actual mass flow rate due to the effect of viscosity in the boundary-layer is $\rho_m u_m \delta_1$. It is interesting to compare some results for this quantity, taking specified values of T_w and T_m, with the approximate results evaluated using a constant fluid property model based on a reference film temperature $T_f = \frac{1}{2}(T_w + T_m)$. The relevant ratio $\rho_m u_m \delta_1/(\rho\delta_1)_f u_m =$ 1·14 and 0·87 for the cases $(T_w, T_m) = (0, 100)$ and (100, 0), respectively.

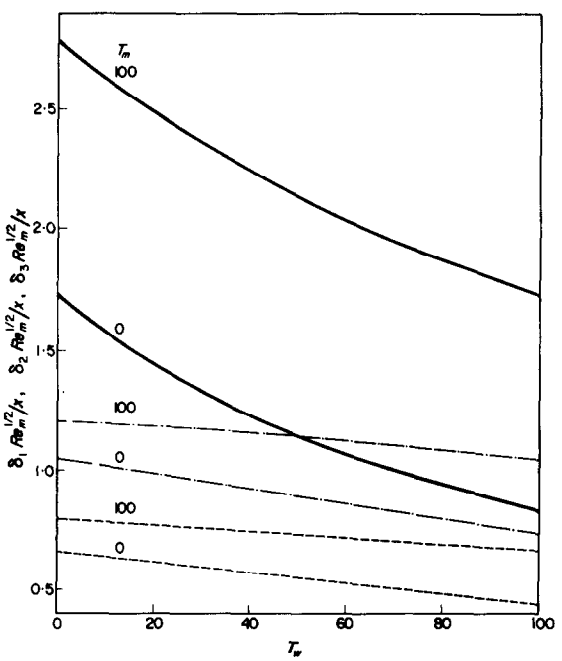

FIG. 3. Boundary-layer thicknesses for the flat plate.
——— $\delta_1 Re_m^{\frac{1}{2}}/x$, -·-·- $\delta_2 Re_m^{\frac{1}{2}}/x$, – – – – $\delta_3 Re_m^{\frac{1}{2}}/x$.

Shear stress

The local shear stress at the plate is:

$$\tau_w = \mu_w\left(\frac{\partial u}{\partial y}\right)_0 = \mu_w \frac{\rho_w}{\rho_m}\left(\frac{\rho_m u_m}{2\mu_m x}\right)^{\frac{1}{2}} u_m f''(0). \qquad (2.22)$$

The related dimensionless skin friction coefficient:

$$C_f = \frac{\mu_w(\partial u/\partial y)_0}{\frac{1}{2}\rho_m u_m^2} = (\sqrt{2})\frac{\rho_w \mu_w f''(0)}{\rho_m \mu_m Re_m^{\frac{1}{2}}}. \qquad (2.23)$$

Values of $C_f Re_m^{\frac{1}{2}}$ are given in Table 1; as expected there is a decrease in $C_f Re_m^{\frac{1}{2}}$ as T_w is increased.

Heat-transfer relations

The characteristic quantity representing the local heat transfer at the plate is $Nu/Re_m^{\frac{1}{2}}$, where the Nusselt number

$$Nu = x\left(\frac{\partial T}{\partial y}\right)_0 \Big/ (T_m - T_w).$$

In terms of the dimensionless temperature

gradient at the plate:

$$Nu/Re_m^{\frac{1}{2}} = \frac{\rho_w}{\rho_m}\frac{\theta'(0)}{\sqrt{2}}; \qquad (2.24)$$

values of this quantity are given in Table 1. The local rate of heat transfer to the plate per unit surface area is given by the relation:

$$q = -k_w(T_m - T_w)\frac{Re_m^{\frac{1}{2}}}{x}\left(\frac{Nu}{Re_m^{\frac{1}{2}}}\right). \qquad (2.25)$$

The method of least squares gives the "best fit" for the data on $Nu/Re_m^{\frac{1}{2}}$ listed in Table 1 as:

$$Nu/Re_m^{\frac{1}{2}} = 0{\cdot}3402\, Pr_m^{0{\cdot}4366}\, Pr_w^{-0{\cdot}09685}, \qquad (2.26)$$

with a r.m.s. error of 0·42 per cent. In the limiting case when $Pr_w = Pr_m$ expression (2.26) reduces to $Nu/Re_m^{\frac{1}{2}} = 0{\cdot}3402\, Pr_m^{0{\cdot}3398}$, which is in reasonable agreement with the classical Blasius–Pohlhausen constant fluid property result $Nu/Re_m^{\frac{1}{2}} = 0{\cdot}3320\, Pr_m^{\frac{1}{3}}$, as given by Eckert and Drake [4]. Using numerical values of the dimensionless temperature gradient $\theta'(0)$ found on integration of (2.15) for $Pr_m = 1(1)14$ gives, for the constant fluid property model, the "best fit" as $Nu/Re_m^{\frac{1}{2}} = 0{\cdot}3334\, Pr_m^{0{\cdot}3394}$, with r.m.s. error of 0·04 per cent.

An alternative approach to the correlation of the theoretical data for $Nu/Re_m^{\frac{1}{2}}$ is to determine effective reference temperatures at which fluid properties should be evaluated when a constant fluid property model is employed. Let the model fluid have an effective reference temperature $T_r = T_w + \gamma(T_m - T_w)$, with $0 \leqslant \gamma \leqslant 1$. It is required to find γ such that:

$$Nu/Re_m^{\frac{1}{2}} \simeq 0{\cdot}3334\, Pr_r^{0{\cdot}3394}, \qquad (2.27)$$

and to make the resulting error as small as possible for all of the various wall and main stream temperatures considered. On performing the necessary computations it was established that the cooled wall data can be represented by (2·27) with $\gamma = 0{\cdot}20$ to within an accuracy of $\pm 1{\cdot}8$ per cent. However, on examination of the heated wall data the most probable value of γ is less than zero and this result is obviously unacceptable. This objection to the use of a constant fluid property model for correlating data on $Nu/Re_m^{\frac{1}{2}}$ is removed by considering correlations involving $Nu/Re_f^{\frac{1}{2}}$, where Re_f is the film Reynolds number. Re-examination of the data yields the result:

$$Nu/Re_f^{\frac{1}{2}} \simeq 0{\cdot}3334 \quad Pr_r^{0{\cdot}3394}, \qquad (2.28)$$

where $\gamma = 0{\cdot}60$ for the heated wall results and $\gamma = 0{\cdot}69$ for the cooled wall results, respectively. The modulus of the resulting error in the use of (2.28) for the particular values of γ was less than 1·5 per cent for the complete range of wall and main stream temperatures considered.

For completeness, the Reynolds analogy factor $Nu/C_f Re_m$ has been included in Table 1.

3. HEAT TRANSFER FROM A ROTATING DISK IN WATER

The axisymmetric laminar flow about a rotating disk situated in a large body of quiescent fluid was first analysed by von Kármán [5] and Cochran [6], using a similarity solution which is a solution both of the full Navier-Stokes equations and of the appropriate boundary-layer equations of the problem. Recently Rogers and Lance [7] have investigated in more detail the general problem of rotationally symmetric flow of a viscous fluid in the presence of an infinite rotating disk.

The heat transfer from such a rotating disk to a model fluid with constant fluid properties has been studied by Millsaps and Pohlhausen [8] for Prandtl numbers in the range

$$0{\cdot}5 \leqslant (c_v/c_p)Pr \leqslant 10;$$

Sparrow and Gregg [9] give numerical results applicable to any Prandtl number. For gases the effects of compressibility were examined by Ostrach and Thorton [10] assuming a model gas with $Pr = 0{\cdot}72$ and a linear variation of viscosity with temperature. A detailed review on the rotating disk and allied mass- and heat-transfer problems has been given by Dorfman [11].

The flow configuration to be studied is that of an infinite circular disk in the horizontal (r, θ)-plane rotating in water with constant

angular velocity Ω about the z-axis. The disk is maintained at uniform surface temperature T_w and the bulk or quiescent fluid is at temperature T_m. As in references [5–10] the relevant similarity solution is given in the form:

$$\left.\begin{aligned} r &= (\mu_m/\rho_m\Omega)^{\frac{1}{2}}R, \\ z &= (\mu_m/\rho_m\Omega)^{\frac{1}{2}}Z, \\ u_r &= (\Omega\mu_m/\rho_m)^{\frac{1}{2}}R\,F(Z), \\ u_\theta &= (\Omega\mu_m/\rho_m)^{\frac{1}{2}}R\,G(Z), \\ u_z &= (\Omega\mu_m/\rho_m)^{\frac{1}{2}}H(Z), \\ p &= \mu_m\Omega\,P(Z), \\ \theta(Z) &= (T - T_w)/(T_m - T_w). \end{aligned}\right\} \quad (3.1)$$

This similarity solution is valid provided the buoyancy force, viscous dissipation and work done against compression are negligible. On examination of the full equations for a viscous heat conducting compressible fluid it can be shown that the effect of the gravitational body force is negligible if:

$$Gr_m/Re_m^{\frac{1}{2}} \ll 1 \quad (3.2a)$$

and, moreover, the effects of viscous dissipation and work done against compression are negligible if:

$$Pr_m\,E_m \ll 1. \quad (3.2b)$$

Occurring in (3.2) are the following dimensionless groups: the Reynolds number $Re_m = \rho_m r^2\Omega/\mu_m$, the modified Grashof number

$$Gr_m = g\frac{\rho_m(\rho_w - \rho_m)r^3}{\mu_m^2},$$

the Eckert number:

$$E_m = \frac{r^2\Omega^2}{Jc_{p_m}(T_w - T_m)}$$

and the Prandtl number $Pr_m = \mu_m c_{p_m}/k_m$.

In terms of the Howarth–Dorodnitsyn variable:

$$\eta = \int_0^z \frac{\rho}{\rho_m}\,dZ, \quad (3.3)$$

and the new variables:

$$f = F, \qquad g = G, \qquad h = \frac{\rho}{\rho_m}H, \quad (3.4)$$

the governing equations expressing conservation of mass, momentum and thermal energy become:

$$2f + h' = 0, \quad (3.5)$$

$$\left(\frac{\mu\rho}{\mu_m\rho_m}f'\right)' = f^2 + hf' - g^2, \quad (3.6)$$

$$\left(\frac{\mu\rho}{\mu_m\rho_m}g'\right)' = 2fg + hg', \quad (3.7)$$

and

$$\left(\frac{\rho k}{\rho_m k_m}\theta'\right)' = Pr_m\frac{c_p}{c_{p_m}}h\theta', \quad (3.8)$$

where the dash denotes differentiation with respect to η. The fluid property relations are given by (2.13). The boundary conditions which must be satisfied at the disk are

$$u_r = 0, \qquad u_\theta = r\Omega, \qquad u_z = 0, \qquad T = T_w$$

and, in terms of the similarity variables (3.1) and the new variables (3.3) and (3.4), these are equivalent to:

$$\begin{aligned} f(0) &= 0, \qquad g(0) = 1, \\ h(0) &= 0, \qquad \theta(0) = 0. \end{aligned} \quad (3.9)$$

At infinity, the fluid has both zero angular and radial velocity and is at constant temperature T_m, hence

$$f(\infty) = 0, \qquad g(\infty) = 0, \qquad \theta(\infty) = 1. \quad (3.10)$$

The dimensionless pressure gradient dP/dZ can be evaluated from the equation:

$$\frac{dP}{dZ} = 2\frac{\rho\mu}{\rho_m\mu_m}f' + \frac{4}{3}\frac{\rho}{\rho_m}\frac{d}{d\eta}\left[\frac{\mu}{\mu_m}(h' - f)\right] - hh'$$

once the solution of the system of differential equations (3.5) to (3.10) is known. However, the actual dynamic pressure change across the

boundary layer is small and of $0(\mu_m\Omega)$ and is therefore negligible within the boundary-layer approximation.

The above similarity solution contains the usual features of boundary-layer theory. The similarity solution is also applicable, within the framework of boundary-layer theory, to the flow in the neighbourhood of the nose of an arbitrary solid of revolution rotating about its axis of revolution in a quiescent fluid; the surface temperature is maintained at $T_w \neq T_m$ the temperature of the fluid, and the axis of symmetry taken to be the vertical axis. In this flow configuration the boundary-layer equations are as given in [3], except that the meridianal momentum equation must include the corresponding component of the gravitational buoyancy force; the pressure along a normal to the surface is now constant. If a is the radius of curvature of the nose the condition for neglecting viscous dissipation is given by (3.2b) with $r = a$; however, the condition for neglecting the gravitational buoyancy force as given by (3.2a) must be replaced by

$$\frac{Gr_m}{Re_m^2} \ll 1,$$

where $r = a$.

The physical interpretation of the constant fluid property flow governed by the Von Kármán similarity solution is well known. The disk acts as a centrifugal pump. At any plane parallel to the disk (and lying within the boundary layer) the fluid is moving in spiral paths away from the central axis of rotation. Consequently, to maintain conservation of mass, there is a uniform normal inflow at the outer edge of the boundary layer. In the following the variable fluid property results obtained for water are now discussed.

Solutions

The seventh-order boundary-value problem (3.5) to (3.10), and including (2.13), has been solved numerically by the method briefly described in Section 2 for $T_w = 0, 10, 40, 70, 100°C$ with $T_m = 0$ and 100°C respectively. The unknown characteristics $f'(0)$, $g'(0)$, $\theta'(0)$ and $h(\infty)$ have been rounded off to four decimals and are listed in Table 2.

Velocity and thermal profiles

Dimensionless velocity and thermal profiles for the cases $(T_w, T_m) = (0, 100), (100, 100), (0, 0)$ and $(100, 0)$ are given graphically in Figs. 4 and 5, respectively; Fig. 6 gives graphically the resultant horizontal velocity

$$u_T = (u_r^2 + u_\theta^2)^{\frac{1}{2}}$$

and its angle

$$\epsilon = \tan^{-1}(u_r/u_\theta)$$

to the zonal direction.

On comparing velocity profiles having the same Reynolds number Re_m it is seen from

Table 2

T_w	T_m	$f'(0)$	$g'(0)$	$\theta'(0)$	$h(\infty)$	$\Delta_1 Re_m^{\frac{1}{2}}/r$	$\Delta_2 Re_m^{\frac{1}{2}}/r$	$\Delta_3 Re_m^{\frac{1}{2}}/r$	$NuRe_m^{-\frac{1}{2}}$	$C_M Re_m^{\frac{1}{2}}/2\pi$
0	100	0·1446	−0·1328	0·5443	−1·0105	0·0664	1·2224	0·2197	0·5681	−0·8790
10		0·1945	−0·1766	0·5391	−1·0023	0·0658	1·1404	0·2140	0·5626	−0·8561
40		0·3109	−0·3225	0·5266	−0·9690	0·0629	0·9370	0·1939	0·5454	−0·7758
70		0·4154	−0·4718	0·5235	−0·9274	0·0587	0·7859	0·1731	0·5343	−0·6924
100		0·5102	−0·6159	0·5278	−0·8845	0·0541	0·6725	0·1540	0·5278	−0·6159
0	0	0·5102	−0·6159	1·2810	−0·8845	0·0541	0·6725	0·1540	1·2810	−0·6159
10		0·6088	−0·7878	1·2836	−0·8660	0·0522	0·6028	0·1442	1·2835	−0·5771
40		0·8586	−1·2770	1·2726	−0·8088	0·0543	0·4483	0·1160	1·2629	−0·4643
70		1·0676	−1·6880	1·2701	−0·7493	0·0383	0·3520	0·0935	1·2418	−0·3744
100		1·2673	−2·0397	1·2862	−0·6933	0·0324	0·2889	0·0770	1·2322	−0·3083

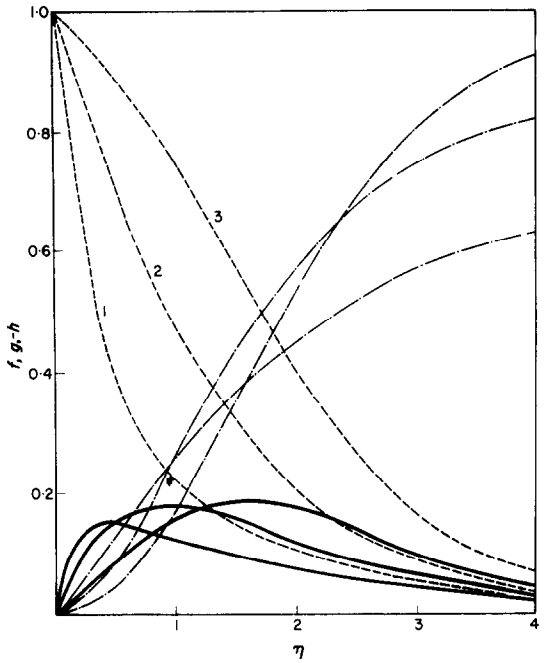

FIG. 4. The velocity functions f, g, h for the rotating disk. ——— f, – – – – g, – · – · – h; 1: $T_w = 100$, $T_m = 0$; 2: $T_w = 0$, $T_m = 0$ or $T_w = 100$, $T_m = 100$; 3: $T_w = 0$, $T_m = 100$.

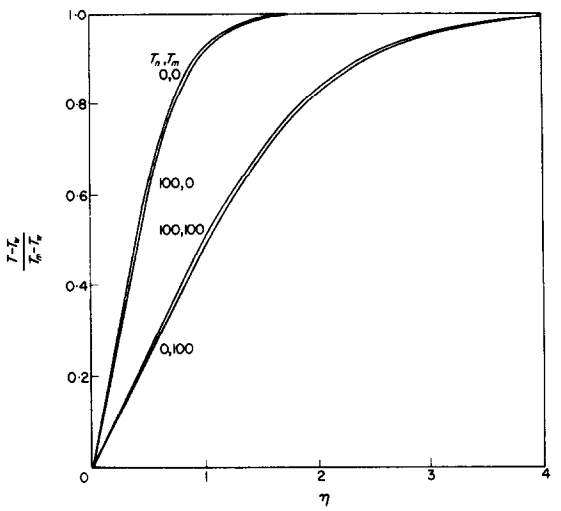

FIG. 5. Dimensionless thermal profiles for the rotating disk.

Fig. 4, for $(T_w, T_m) = (0, 0)$ and (100, 0), that an increase in the disk temperature produces a decrease in zonal velocity. Obviously heating the disk reduces the viscosity and so causes a reduction in the zonal component of the shearing stress exerted by the disk on the neighbouring layer of fluid. Consequently, there is a reduction in the centrifugal force induced by the disk resulting in a reduction in the radial component of velocity and also in the axial inflow at the edge of the boundary layer. The resultant horizontal velocity component, as seen from Fig. 6, is now obviously decreased on supplying

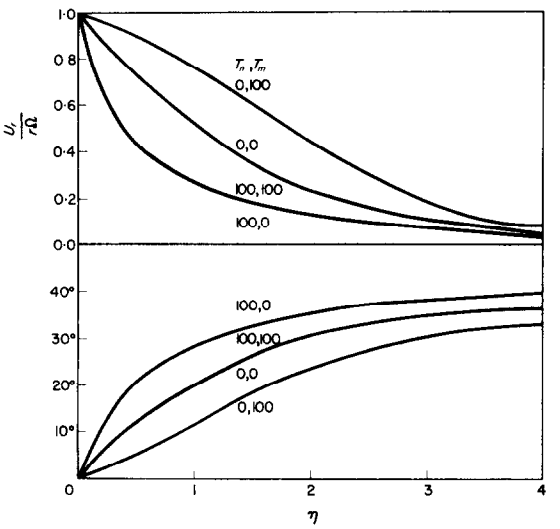

FIG. 6. Dimensionless tangential velocity $U_T/r\Omega$ and angle ϵ.

heat to the disk; moreover, the angle ϵ is increased producing a more diffuse spiral motion. Returning to Fig. 4 it is significant that as heat is supplied to the disk the maximum radial velocity, although reduced slightly in magnitude, is located closer to the disk. Near the disk heating produces a slight increase in axial inflow, whereas at the outer edge of the boundary layer there is an appreciable decrease since the latter is controlled by the overall reduction in radial outflow.

As seen from Fig. 5 the dimensionless thermal profiles for the cases $(T_w, T_m) = (0, 0)$, (100, 0) nearly coalesce. This implies that wall heat-transfer coefficients for the rotating disk are insensitive to changes in T_w for fixed T_m. Clearly from equation (3.8) the shape or exponential

decay of these profiles is determined primarily by the fixed magnitude of Pr_m. The observed small decrease with increasing T_w is evidently due to minor local variations of the inflow near to the disk.

Briefly, the actual trends, as in the cases (T_w, T_m) = (100, 100), (0, 100), for cooling the disk are as follows. Cooling produces an increase in the zonal shear stress at the disk leading to increased radial outflow balanced by a corresponding increase in the inflow. As seen from Fig. 6 there are associated increases in the resultant horizontal component of velocity and moreover the spiral motion becomes more compact. Once again the thermal profiles are controlled by Pr_m and are insensitive to changes in T_w.

Note that the mass of fluid pumped outwards from one side of the disk per second (across a semi-infinite cylinder of radius r, $z \geqslant 0$) as a result of the centrifugal effect is

$$Q = 2\pi r \int_0^\infty \rho u_r \, d\eta = \pi r^3 \rho_m \Omega Re_m^{-\frac{1}{2}} [-h(\infty)]. \quad (3.11)$$

This quantity is also the actual mass flow per second which flows axially towards the disk.

Boundary-layer thicknesses

The following dimensionless length scales have been evaluated as measures of the fluid boundary-layer thickness on the rotating disk. These are:

$$\Delta_1 = \int_0^\infty \frac{\rho u_r^2}{\rho_m \Omega^2 r^2} d\eta = r Re_m^{-\frac{1}{2}} \int_0^\infty f^2 \, d\eta, \quad (3.12)$$

$$\Delta_2 = \int_0^\infty \frac{\rho u_\theta^2 / r}{\rho_m \Omega^2 r} d\eta = r Re_m^{-\frac{1}{2}} \int_0^\infty g^2 \, d\eta, \quad (3.13)$$

and

$$\Delta_3 = \int_0^\infty \frac{\rho u_r u_\theta}{\rho_m r^2 \Omega^2} d\eta = r Re_m^{-\frac{1}{2}} \int_0^\infty fg \, d\eta. \quad (3.14)$$

They are in fact associated with the total rate of change of radial momentum across a cylinder of radius r, the centrifugal force at radius r and the rate of change of zonal momentum at radius r, respectively. Numerical values of $\Delta_1 Re_m^{\frac{1}{2}}/r$, $\Delta_2 Re_m^{\frac{1}{2}}/r$, $\Delta_3 Re_m^{\frac{1}{2}}/r$ are given in Table 2. As expected, these quantities decrease with increasing T_w for fixed T_m and Re_m.

Torque and moment coefficient

The approximate torque on a finite disk of radius r is now evaluated. The torque on one side is:

$$M = -2\pi \int_0^r r^2 \tau_{z\theta} \, dr, \quad (3.15)$$

where the zonal shear stress is:

$$\tau_{z\theta} = \mu_w \left(\frac{\partial u_\theta}{\partial \eta} \right)_{\eta = 0}.$$

The dimensionless moment coefficient is defined as

$$C_M = \frac{2M}{\frac{\rho_m}{2} \Omega^2 r^5} = 2\pi Re_m^{-\frac{1}{2}} \frac{(\rho\mu)_w}{(\rho\mu)_m} g'(0). \quad (3.16)$$

Values of $C_M Re_m^{\frac{1}{2}}/2\pi$ are given in Table 2. When $T_m = 0°C$ and Re_m is fixed there is an overall decrease of 50 per cent in C_M as T_w increases from 0 to 100°C.

Nusselt number

The Nusselt number is defined as:

$$Nu = r \left(\frac{\partial T}{\partial z} \right)_{z=0} / (T_w - T_m).$$

The characteristic quantity

$$Nu/Re_m^{\frac{1}{2}} = \frac{\rho_w}{\rho_m} \theta'(0)$$

is given in Table 2.

The method of least squares gives the "best fit" for this data as:

$$Nu/Re_m^{\frac{1}{2}} = 0{\cdot}4187 \, Pr_w^{0{\cdot}02861} \, Pr_m^{0{\cdot}4048} \quad (3.17)$$

with a r.m.s. error of 0·22 per cent. for the constant

fluid property model using T_m as the reference temperature and computed solutions for $Pr_m = 1(1)14$ the "best fit" was:

$$Nu/Re_m^{\frac{1}{2}} = 0{\cdot}4127\, Pr_m^{0{\cdot}4404} \qquad (3.18)$$

with a r.m.s. error of 0·45 per cent. The result (3·17) is in good agreement with (3.18) when $Pr_w = Pr_m$. Note that (3.17) indicates the weak dependence of $Nu/Re_m^{\frac{1}{2}}$ on Pr_w.

Finally reference temperatures are proposed, as in Section 2, for a related constant fluid property model. The variable fluid property data for $Nu/Re_f^{\frac{1}{2}}$ can be evaluated using constant fluid property results, namely,

$$Nu/Re_f^{\frac{1}{2}} \simeq 0{\cdot}4127\, Pr_r^{0{\cdot}4404}, \qquad (3.19)$$

where property values are taken at

$$T_r = T_w + \gamma(T_m - T_w)$$

with $\gamma = 0{\cdot}41$ for the heated wall and $\gamma = 0{\cdot}44$ for the cooled wall, respectively. The modulus of the maximum error involved in the use of (3.19) for both values of γ was less than 0·3 per cent for the particular wall and main stream temperatures considered.

4. CONCLUDING REMARKS

In the previous two sections results have been obtained on the effects of variable fluid properties on flow and heat transfer in water. These solutions of the laminar boundary-layer equations are in fact variable fluid property generalizations of well known constant fluid property similarity solutions. Section 2 has now been extended to include solutions of the laminar layer equations with an adverse pressure gradient. By numerical integration of the relevant partial differential equations it is hoped to present information on the effect of variable fluid properties on non-isothermal laminar flows with boundary-layer separation.

REFERENCES

1. G. Poots and M. H. Rogers, Laminar flow between parallel flat plates, with heat transfer, of water with variable physical properties, *Int. J. Heat Mass Transfer* **8**, 1515 (1965).
2. Y. R. Meyhew and G. F. C. Rogers, *Thermodynamic and Transport Properties of Fluids* (MKS Units). Blackwell, Oxford (1964).
3. K. Stewartson, *The Theory of Laminar Boundary Layers in Compressible Fluids*. Oxford Mathematical Monographs, Clarendon Press, Oxford (1964).
4. E. R. G. Eckert and R. M. Drake, *Heat and Mass Transfer*. McGraw Hill, New York (1959).
5. Th. Von Kármán, Über laminare und turbulente Reibung, *Z. Angew Math. Mech.* **1**, 233 (1921).
6. W. G. Cochran, The flow due to a rotating disc, *Proc. Camb. Phil. Soc.* **30**, 365 (1934).
7. M. H. Rogers and G. N. Lance, The rotationally symmetric flow of a viscous fluid in the presence of an infinite rotating disk, *J. Fluid Mech.* **7**, 617 (1960).
8. K. Millsaps and K. Pohlhausen, Heat transfer by laminar flow from a rotating plate, *J. Aeronaut. Sci.* **19**, 120 (1952).
9. E. M. Sparrow and J. L. Gregg, Heat transfer from a rotating disk to fluids of any Prandtl number, *J. Heat Transfer*, **81C**, 249 (1959).
10. S. Ostrach and P. R. Thorton, Compressible laminar flow and heat transfer about a rotating isothermal disk, NACA TN 4320 (1954).
11. L. A. Dorfman, *Hydrodynamic Resistance and the Heat Loss of Rotating Solids*. Oliver and Boyd, Edinburgh (1963).

Résumé—On présente des solutions numériques pour la convection forcée laminaire de la chaleur dans de l'eau pour deux configurations différentes de couche limite laminaire. On emploie les valeurs expérimentales (dans la gamme de 0–100°C) pour la viscosité, la conductivité, la chaleur spécifique et la masse volumique. On examine d'abord le transport de chaleur par convection forcée laminaire à partir d'une plaque plane semi-infinie vers un écoulement parallèle. On alyse ensuite le transport de chaleur par écoulement laminaire au voisinage d'un disque tournant infini. On suppose que la dissipation par viscosité, le travail de compression et la force volumique due à la pesanteur sont négligeables. Les équations correspondantes de la couche limite sont résolues numériquement pour des conditions de plaque (ou de disque) isotherme.

Les propriétés d'écoulement et de transport de chaleur de ces solutions sont données, pour les deux régimes d'écoulement, sous forme de graphiques et de tableaux pour plusieurs combinaisons de températures de plaques et d'écoulement libre. Les résultats théoriques pour le nombre de Nusselt pariétal sont représentés par des expressions du type:

$$Nu/Re^{\frac{1}{2}} = APr_w^{\alpha} Pr_m^{\beta},$$

où Re est le nombre de Reynolds, Pr est le nombre de Prandtl et les indices inférieurs m et w indiquent que l'on a pris les valeurs des propriétés du fluide dans l'écoulement principal et à la paroi. On tiendra compte aussi de l'emploi de températures de référence effectives auxquelles les propriétés du fluide devraient être calculées lorsqu'on utilise un modèle à propriétés constantes de fluide pour déterminer les coefficients de transport de chaleur à la paroi.

Zusammenfassung—Numerische Lösungen werden angegeben für den Wärmeübergang bei laminarer Zwangskonvektion in Wasser, bei verschiedenen Anordnungen der laminaren Grenzschichtströmung. Für die Zähigkeit, die Leitfähigkeit, die spezifische Wärme und die Dichte werden Versuchswerte (im Bereich 0–100°C verwendet. Erstens wird der Wärmeübergang bei laminarer Zwangskonvektion an einer halbunendlichen, ebenen Platte, die parallel aggeströmt wird, untersucht. Zweitens der Wärmeübergang bei laminarer Strömung an einer unendlichen rotierenden Scheibe analysiert. Es wird angenommen, dass die Dissipationsfunktion, die Kompressionsarbeit und der Auftrieb vernachlässigbar sind. Die entsprechenden Grenzschichtgleichungen werden numerisch für die isotherme Platte (oder Scheibe) gelöst.

Die Strömungs- und Wärmeübergangseigenschaften dieser Lösungen beider Strömungsformen sind in Diagrammen und Tabellen für verschiedene Kombinationen von Platten und Freistromtemperaturen wiedergegeben. Die theoretischen Ergebnisse für die Nusseltzahl sind durch Ausdrücke von der Art $Nu/Re^{\frac{1}{2}} = A\,Pr_w^a\,Pr_m^b$ korreliert, wobei Re die Reynoldszahl und Pr die Prandtlzahl darstellt, und die Indices m und w angeben, ob die Eigenschaften des Hauptstromes oder der Wand zugrundegelegt sind. Ebenfalls berücksichtigt wurden effektive Bezugstemperaturen, bei welchen die Stoffwerte der Flüssigkeit einzusetzen sind, wenn zur Bestimmung der Wärmeübergangskoeffizienten ein Modell konstanter Flüssigkeitstemperatur verwendet wird.

Аннотация—Представлены численные решения для двух ламинарных пограничных слоев различной конфигурации при вынужденной конвекции в потоке воды. Используются экспериментальные значения (в диапазоне 0–100°C) вязкости, теплопроводности, удельной теплоты и плотности. Во-первых, исследовался перенос тепла в ламинарном потоке при вынужденной конвекции от полубесконечной плоской пластины к параллельному потоку. Во-вторых, анализировался перенос тепла ламинарным потоком на бесконечном вращающемся диске. Предполагается, что можно пренебречь вязкой диссипацией, сжимаемостью потока и гравитационной подъемной силой. Численно решены соответствующие уравнения пограничного слоя для пластины (или диска) при изотермических условиях.

Эти решения для обоих режимов потока представлены в виде графиков и таблиц при различных комбинациях температур пластины и свободного потока. Теоретические результаты для числа Нуссельта на стенке описываются следующими выражениями $Nu/Re^{\frac{1}{2}} = A\,Pr_w^a\,Pr_m^\beta$, где Re — число Рейнольдса; Pr — число Прандтля и индексы m, w — показывают, что свойства жидкости взяты при температуре основного потока или стенки, соответственно. Также рассматривается использование эффективных температур, при которых нужно определять характеристики потока жидкости при использовании модели постоянных свойств жидкости для определения коэффициентов теплообмена на стенке.